



PAPER • OPEN ACCESS

## 3D bioprinting of *E. coli* MG1655 biofilms on human lung epithelial cells for building complex *in vitro* infection models

To cite this article: Samy Aliyazdi *et al* 2023 *Biofabrication* **15** 035019

View the [article online](#) for updates and enhancements.

### You may also like

- [From molecules to multispecies ecosystems: the roles of structure in bacterial biofilms](#)  
Vernita Gordon, Layla Bakhtiari and Kristin Kovach
- [Material properties of biofilms—a review of methods for understanding permeability and mechanics](#)  
Nicole Billings, Alona Birjiniuk, Tahoura S Samad *et al.*
- [3D bioprinting of mature bacterial biofilms for antimicrobial resistance drug testing](#)  
Evita Ning, Gareth Turnbull, Jon Clarke *et al.*

# Biofabrication



## PAPER

### OPEN ACCESS

RECEIVED  
18 January 2023

REVISED  
25 April 2023

ACCEPTED FOR PUBLICATION  
26 May 2023

PUBLISHED  
6 June 2023

Original content from this work may be used under the terms of the [Creative Commons Attribution 4.0 licence](https://creativecommons.org/licenses/by/4.0/).

Any further distribution of this work must maintain attribution to the author(s) and the title of the work, journal citation and DOI.



# 3D bioprinting of *E. coli* MG1655 biofilms on human lung epithelial cells for building complex *in vitro* infection models

Samy Aliyazdi<sup>1,3</sup> , Sarah Frisch<sup>1,3</sup> , Alberto Hidalgo<sup>1,4</sup> , Nicolas Frank<sup>2</sup> , Daniel Krug<sup>2,3</sup> , Rolf Müller<sup>2,3</sup> , Ulrich F Schaefer<sup>3</sup> , Thomas Vogt<sup>5</sup> , Brigitta Loretz<sup>1,3</sup> and Claus-Michael Lehr<sup>1,3,\*</sup>

<sup>1</sup> Department of Drug Delivery, Helmholtz Center for Infection Research, Helmholtz-Institute for Pharmaceutical Research Saarland, Campus E8 1, 66123 Saarbrücken, Germany

<sup>2</sup> Department of Microbial Natural Products, Helmholtz Center for Infection Research, Helmholtz-Institute for Pharmaceutical Research Saarland, Campus E8 1, 66123 Saarbrücken, Germany

<sup>3</sup> Saarland University, 66123 Saarbrücken, Germany

<sup>4</sup> Charite-Universitätsmedizin Berlin, Institute of Functional Anatomy, Philippstraße 12, 10115 Berlin, Germany

<sup>5</sup> University Clinic Homburg, Clinic for Dermatology, Kirrberger Str., 66424 Homburg, Germany

\* Author to whom any correspondence should be addressed.

E-mail: [claus-michael.lehr@helmholtz-hips.de](mailto:claus-michael.lehr@helmholtz-hips.de)

**Keywords:** 3D printing, hydrogel, antimicrobial resistance, alternatives to animal experiments, chronic lung infections

Supplementary material for this article is available [online](#)

## Abstract

Biofilm-associated infections are causing over half a million deaths each year, raising the requirement for innovative therapeutic approaches. For developing novel therapeutics against bacterial biofilm infections, complex *in vitro* models that allow to study drug effects on both pathogens and host cells as well as their interaction under controlled, physiologically relevant conditions appear as highly desirable. Nonetheless, building such models is quite challenging because (1) rapid bacterial growth and release of virulence factors may lead to premature host cell death and (2) maintaining the biofilm status under suitable co-culture requires a highly controlled environment. To approach that problem, we chose 3D bioprinting. However, printing living bacterial biofilms in defined shapes on human cell models, requires bioinks with very specific properties. Hence, this work aims to develop a 3D bioprinting biofilm method to build robust *in vitro* infection models. Based on rheology, printability and bacterial growth, a bioink containing 3% gelatin and 1% alginate in Luria-Bertani-medium was found optimal for *Escherichia coli* MG1655 biofilms. Biofilm properties were maintained after printing, as shown visually via microscopy techniques as well as in antibiotic susceptibility assays. Metabolic profile analysis of bioprinted biofilms showed high similarity to native biofilms. After printing on human bronchial epithelial cells (Calu-3), the shape of printed biofilms was maintained even after dissolution of non-crosslinked bioink, while no cytotoxicity was observed over 24 h. Therefore, the approach presented here may provide a platform for building complex *in vitro* infection models comprising bacterial biofilms and human host cells.

## 1. Introduction

It is estimated that biofilm associated infections are causing half a million deaths each year in the US alone, with an economic burden of annually \$94 billion [1, 2]. This raises the requirement for novel therapeutic approaches against biofilm infections. Bacterial biofilms are populations of bacteria that live in self-produced protective extracellular matrices (ECMs) composed of proteins, polysaccharides and

nucleic acids [3]. The ability of many bacteria to produce biofilms is associated with chronic infections and antibiotic resistance, thus causing a serious health burden via a variety of mechanisms [4–6]. Key aspects include the creation of a penetration barrier against many antibiotic molecules, an altered chemical microenvironment or subpopulation of microorganisms, leading to therapy failures [4, 7]. Biofilms can form on many different surfaces and tissues [8]. For example, biofilm related lung infection, mediated

by *Pseudomonas aeruginosa* (*P. aeruginosa*) in patients suffering from cystic fibrosis, is one of the most common associated diseases [9, 10]. There, the pathogen forms biofilms on lung epithelium due to impaired mucociliary clearance [10].

The discovery of novel anti-infective compounds as well as their subsequent preclinical development requires robust biofilm models for fast testing purposes. The gold-standard approach is still animal models, including rats, mice, cats and many more, which are infected intratracheally or intranasally with bacteria loaded agar-beads [11]. However, interspecies differences in anatomy, genetics and immunology show suboptimal properties of animal models with human pathogenic bacteria in representation of comparable pathology. *In vitro* alternatives, ideally with co-cultures of human epithelial cells and bacterial biofilms, exist but are still limited in flexibility and cultivability.

Anderson *et al* attempted to cultivate *P. aeruginosa* biofilms on epithelial lung cells. However, the cells died rapidly during the biofilm formation process after 4–6 h [12]. Similar observations were made by Woodworth *et al*, who associated accelerated cell death with biofilm production [13]. Another study indicated that human *in vitro* cell systems were more prone to rapid cell death in the presence of planktonic bacteria due to massive overgrowth, than in the presence of a pre-established biofilm with reduced metabolism [14]. Montefusco-Pereira *et al* established a model with planktonic bacteria for anti-infective testing, which was treated 1 h after cell infection to prevent prompt cell death [15]. More recent approaches, such as those by Horstmann *et al* and Juntke *et al* involved transferring separately pre-grown biofilms onto human cell monolayers [16, 17]. By administering antibiotics repeatedly, such mixed cultures of bacteria and human cells could remain viable for 72 h under air–liquid conditions.

However, a major drawback of the aforementioned approaches is the poor control of the transferred biofilms.

A method to shape and transfer biofilms in a controllable manner could be the emerging technology of 3D bioprinting, a technique to fabricate and shape living materials like cells inside of hydrogels. This led to innovations in tissue engineering and regenerative medicine. Bone tissue [18], cardiac tissue [19, 20], liver tissue [21], skin tissue [22] and many other tissues [23] were already bioprinted successfully. Recently, the approach was applied to bioprint also living bacteria for different biotechnological and biomedical purposes [24, 25], including fabrication of bacterial biofilms. Spiesz *et al* and Balasubramanian *et al* bioprinted planktonic *Escherichia coli* MG1655 (*E. coli* MG1655) in an alginate solution on CaCl<sub>2</sub>-Luria-Bertani (LB)-agar plates, which were incubated for 3–6 d to form a biofilm within the shape [26, 27].

Similarly, Ning *et al* bioprinted *E. coli*, *Staphylococcus aureus* (*S. aureus*) and *P. aeruginosa* biofilms for antimicrobial testing. They mixed the planktonic bacteria with partially crosslinked alginate and printed them on plastic surfaces. The biofilm was then formed within the printed construct after 5–14 d, depicted via fluorescence imaging [28]. However, their approach would not be suitable to print bacterial biofilms on human epithelial cells, e.g. to mimic a biofilm related infection model, because if printed on cells directly, the biofilms are not formed yet and the transfer of the 5–14 d old crosslinked constructs are not optimal for any fine shapes.

In this work, we demonstrate a novel method to print biofilms, using *E. coli* as a model strain. For that, we tested and characterized gelatin-alginate hydrogels with different polymer concentrations to find the optimal bioink base for printing bacteria on epithelial cells. For this purpose, biofilms were firstly grown in the selected hydrogels and subsequently printed in different shapes. To assure that biofilm properties are maintained after bioprinting antibiotic susceptibility assays, metabolic profile analysis and microscopy techniques were performed and compared to native biofilms and planktonic bacteria. To check cell biocompatibility and whether biofilms can be shaped on human *in vitro* systems, biofilms were printed on top of confluent human bronchial epithelial (Calu-3) cell monolayers.

## 2. Material and methods

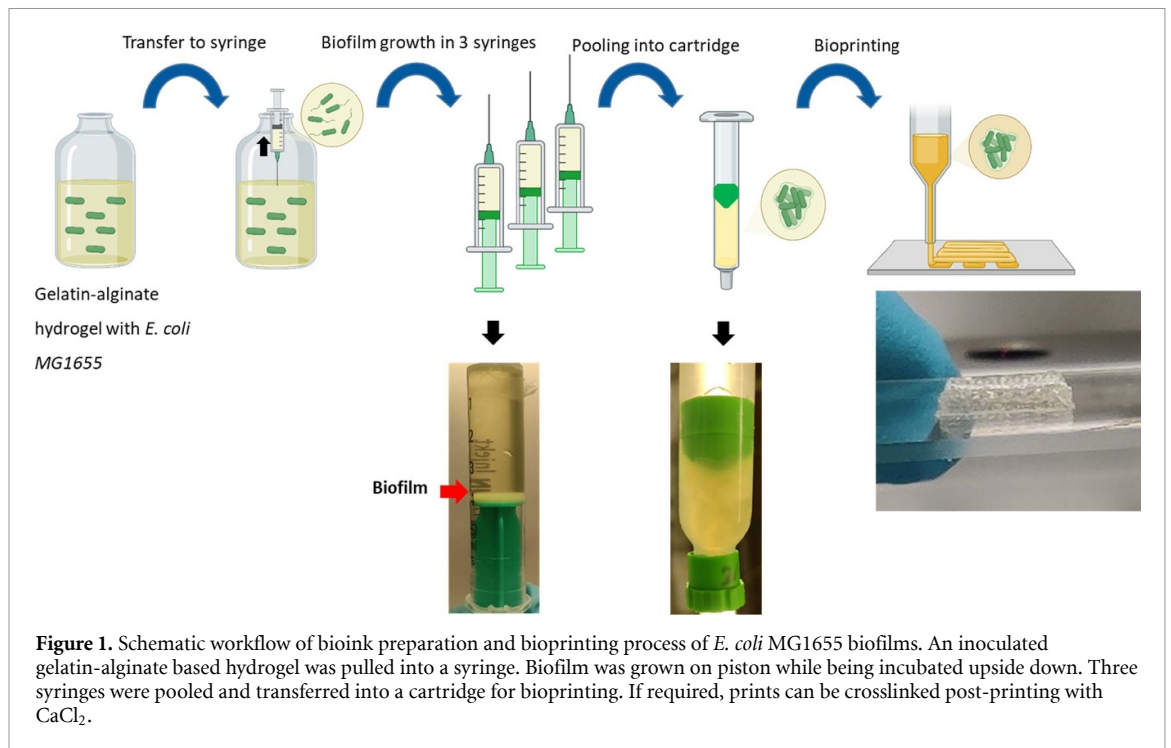
### 2.1. Bacterial and human cell culture

*E. coli* MG1655 was selected as a model strain, due to its ability to form biofilms and its ease of culturing as a S1 strain. *E. coli* MG1655 was cultured on LB-agar plates, streaked from frozen glycerol stocks. An overnight (O/N) culture was initiated by inoculating a single colony into an Erlenmeyer flask containing 25 ml LB-medium (Sigma-Aldrich, Germany) and incubating it shaking (180 rpm) at 37 °C.

Calu-3 cells (HTB-55, ATCC, LGC Germany) were chosen as an epithelium lung cell model. They were cultured in minimum essential medium (Gibco, UK) in cell culture flasks (Greiner, Germany), supplemented with 10% fetal bovine serum (Gibco, UK), 1% sodium pyruvate (Gibco, USA) and 1% Non-Essential Amino Acids (NEAA, Gibco, UK). Cells were kept at 37 °C at 5% CO<sub>2</sub> and medium was exchanged every 2–3 d. Passaging was performed once per week.

### 2.2. Bioink preparation

Gelatin (Bloom 300, Type A, Sigma-Aldrich, Germany) and sodium alginate (W202503, Sigma-Aldrich, Germany) were weighed at different concentrations in 12 ml of LB medium and stirred at 60 °C–70 °C for solvation. Immediately, the solutions were



sterile filtered (0.45  $\mu\text{m}$  pore size) in 50 ml falcons and stored at 4 °C. For inoculation, the hydrogel was liquefied at 37 °C and 10 ml was transferred to two sterile vials. The following steps are generalized in figure 1. An aliquot of *E. coli* MG1655 O/N culture was measured for the  $\text{OD}_{600}$  and diluted to contain  $10^6$  CFU  $\text{ml}^{-1}$ . A 100  $\mu\text{l}$  of the aliquot was added to each 10 ml bioink sample. The suspension was briefly stirred and then 5 ml plus  $\sim 1$  ml air were pulled up into three syringes. Syringes were covered with sterile parafilm and then incubated upside down in Erlenmeyer flasks at 37 °C for 3 d. During this incubation period, the biofilm primarily forms on the surface of the syringe plunger. Then, 4 ml of all three suspensions above the grown biofilms were discarded carefully by a second empty syringe, pushing the supernatant up via a female luer lock adapter. The remaining 1 ml of those three suspensions were pooled carefully from syringe to syringe, with the biofilm detaching from the plungers when pushed out. Then, the bioink was transferred gently to a sterile cartridge. Subsequently, the bioink was slowly rotated (3 rpm, Multi-Rotator PTR-35, Grant, UK) for 3–4 h to prevent sedimentation until the hydrogel solidifies at exactly 21 °C.

As controls, native biofilms and the bioink with dispersed planktonic bacteria were used. Native biofilms were prepared by growing  $10^5$  CFU  $\text{ml}^{-1}$  bacteria in 5 ml LB medium in polystyrene 6-well plates for 3 d at 37 °C, covered with parafilm. In the case of bioink with planktonic bacteria, the cell amount was maintained equal by determining the CFU of the biofilm bioink before. For that, 85 mg of the bioink was solved in 1 ml PBS, vortexed for

10 min (to detach clumps) and plated on LB-agar plates via serial dilution in PBS. A CFU  $\text{ml}^{-1}$  of  $10^{10}$  was then calculated by the bioinks density ( $957.3 \pm 0.9$  mg  $\text{ml}^{-1}$  via weighing). Then, an *E. coli* MG1655 O/N culture (O/N stirred  $\rightarrow$  avoids biofilm aggregations) was concentrated twice by centrifugation at 5000 rpm and the pellet was resuspended first in 2 ml and then in 200  $\mu\text{l}$  ( $10^{12}$  CFU  $\text{ml}^{-1}$ ). Then 100  $\mu\text{l}$  was added into two vials filled with 10 ml of the hydrogel at a final concentration of  $10^{10}$  CFU  $\text{ml}^{-1}$ . Thereafter, 5 ml of the bioink was pulled up into a syringe and transferred to a cartridge via a female luer lock adapter. The cartridge was then rotated.

Native planktonic bacteria were also dispersed in LB medium as stated in methods section 2.7.

### 2.3. Rheological analysis

For rheological characterization  $\sim 100$   $\mu\text{l}$  of either bioink dispersions was transferred from the cartridge to a syringe via a Luer lock adapter and extruded on a 20 mm parallel Peltier steel plate of a rheometer (Discovery Hybrid, Waters/TA Instruments, Germany). All measurements were conducted at 21 °C. Oscillation amplitude analysis was performed at 1 Hz with a range of 0.01%–1000% strain. Oscillation frequency was performed with 1% strain from 0.1 to 10 Hz. Flow Sweep was performed with shear rate ranging from 1  $\text{s}^{-1}$  to 100  $\text{s}^{-1}$ .

### 2.4. Printability

Printability of bioinks was characterized via a 3D bioprinter (3D Discovery, RegenHu, Villaz ST-Pierre, Switzerland). A 25 G needle was mounted to the cartridges, which were then connected to an air

pressure source for filament extrusion. To evaluate printability, a solid construct with five layers was printed and weighed. For each bioink, the air pressure was adjusted to achieve a construct weight of 85 mg. This procedure was repeated for all experiments to ensure consistent bioink volume extrusion. All pressure measurements were performed in biological triplicates. Additionally, different shapes and dimensions of prints were fabricated with the selected bioink, designed via the bioprinter's specific software (BIOCAD™), to show bioprinting versatility. To obtain a rapid assessment of viability, we printed bioinks onto LB-agar plates and incubated them O/N at 37 °C.

### 2.5. Fluorescent microscopy of bacteria

Constructs (two layers to avoid signal reduction in higher depths) were printed in a 12 well plate and crosslinked with 2 ml 100 mM CaCl<sub>2</sub> for 15 min. Crosslinking was necessary to prevent shape disruption during the staining protocol. Afterwards, the solutions were discarded, and 1 ml of PBS was added. Then, 3 μl BacLight™ staining solution, consisting of a 1:1 mixture of SYTO 9 (488 nm excitation, green emission) and propidium iodide (490 nm excitation, red emission) was added. Bacteria were stained for 15–20 min in the dark. As controls, native biofilms were prepared as described and stained accordingly with 15 μl BacLight™ staining solution in the medium to avoid biofilm disruption. Native planktonic bacteria were prepared as previously described, with 90 μl of the 10<sup>10</sup> CFU ml<sup>-1</sup> suspension added to 1 ml of PBS in a 12 well plate. Next, bacteria were stained with 3 μl BacLight™. Bacteria were then imaged at a fluorescence microscope (confocal laser scanning microscope (CLSM), Leica DMI8, Germany), using a 10× objective (HC PL Fluotar 10×/0.3 Dry, Leica, Germany) and the LAS X software. Triplicates of all samples were imaged, each at 2–3 different and random *xyz* positions, providing a strong fluorescent signal. All images were collected, using equal parameters, including gain and laser intensity to ensure comparability.

### 2.6. Scanning electron microscope (SEM) analysis of printed bacteria

Three percent glutaraldehyde were added to cover printed and crosslinked (as stated in section 2.5) biofilms and planktonic bacteria for 90 min. Then, an ethanol dilution series ranging from 30% to 100% (10 min incubation time for each concentration) was added to the prints. Finally, hexamethyldisilazane was added to the prints for another 10 min. The solution was removed, and constructs were kept at room temperature (RT) O/N. Prints were attached to SEM sample holder via adhesive carbon tabs (Plano, Germany) and then gold sputtered for 100 s and analyzed at a SEM (EVO HD15, Zeiss, Germany). Native

counterparts were not included, due to transferability issues to the SEM samples holders.

### 2.7. Antibiotic susceptibility

Five layers of non-porous 8 × 8 mm squares of biofilm and planktonic bioink were printed in triplicates into 12 well plates. As control samples native biofilms and native planktonic bacteria were prepared as described previously. Bioprinted bioinks were crosslinked for 15 min at RT with 100 mM CaCl<sub>2</sub> solution. Crosslinking agents were removed and 2 ml LB-medium (untreated control) or antibiotic solution in LB medium was added. The antibiotics used were ampicillin (128 μg ml<sup>-1</sup>; Roth, Germany), tetracycline hydrochloride (4 μg ml<sup>-1</sup>; Chemodex, Switzerland), colistin sulfate (16 μg ml<sup>-1</sup>; Adipogen, Switzerland) and ciprofloxacin hydrochloride (0.5 μg ml<sup>-1</sup>; Sigma-Aldrich, Germany). Same antibiotic treatments were applied for native biofilms and printed planktonic bacteria. For native planktonic bacteria, an O/N culture was set to 10<sup>10</sup> CFU ml<sup>-1</sup> and 90 μl (equaled weight of printed constructs) was added to 2 ml of antibiotic solution. After an O/N incubation, printed constructs were washed twice with PBS and then solved in 1 ml ethylenediaminetetraacetic acid (EDTA, 110 mM, Roth, Germany). For CFU determination, serial dilution was prepared in PBS and then plated on LB-agar plates (3 × 20 μl drops per dilution). Log CFU ml<sup>-1</sup> was set to 1 when no colonies were grown.

Native biofilms were quickly vortexed in falcons and then 90 μl were diluted in 1 ml of PBS. After serial dilution in PBS, suspensions were plated accordingly.

For native planktonic bacteria, suspensions were vortexed quickly and diluted 1:10 in 1 ml PBS accordingly. After serial dilution in PBS, suspensions were plated.

### 2.8. Metabolic profile comparison

Bioink with planktonic and biofilm bacteria, respectively, were printed and dissolved in 1 ml LB medium at 37 °C. Accordingly, native biofilm bacteria and planktonic bacteria were prepared and collected into 15 ml falcons. Then, 90 μl was transferred into 1 ml of LB medium. All bacterial suspensions were transferred into Eppendorf tubes and centrifuged at 5000 rpm. Supernatants were discarded. For medium control subtraction, 1 ml of LB medium and plain hydrogel (for native samples and for printed samples respectively) were centrifuged accordingly, and supernatants were discarded. Since these samples yielded no pellet, the tiny remaining liquids after supernatants' discarding were used. Afterwards, sample preparation and LC-TOF measurements were performed following the protocol of Montefusco-Pereira *et al* [15]. Briefly, 1 ml of methanol was added plus 25 ng sulfadimidine as an internal standard, which was then vortexed for

10 min. The 100  $\mu\text{l}$  methanol was added to the pellets. LC-TOF measurements were then conducted on a Thermo Dionex Ultimate 3000 RSLC system coupled to a Bruker maXis 4G UHR-Q-TOF-MS. The separation process was performed via an 18 min linear 5%–95% gradient of acetonitrile with 0.1% formic acid (B) in ddH<sub>2</sub>O with 0.1% formic acid (A) on a Waters Acquity BEH C18 column (100  $\times$  2.1 mm, 1.7  $\mu\text{m}$  dp) at a flow rate of 0.6 ml min<sup>-1</sup> and 45 °C. The LC flow was split to 75  $\mu\text{l}$  min<sup>-1</sup> before entering the mass spectrometer. Mass spectra were acquired in centroid mode ranging from 150 to 2500  $m/z$  at a 2 Hz scan rate. Statistical non-targeted metabolomics analysis was performed with MetaboScape 9.0.1 (Bruker Daltonics). The minimal intensity threshold for peak detection was set to  $2.5 \times 10^3$  with a maximum charge state of 3. Retention time alignment to match features between different samples was automatically performed by the feature extraction algorithm. For every condition, 9 replicates were generated and measured twice, resulting in a total number of 18 replicates. Features were only reported if they appeared in at least 18 samples in total and at least 1 replicate of the same condition. After generating a feature table in MetaboScape, all blank features were subtracted from the analysis resulting in a data reduction of 87%. The final data are depicted in feature tables representing the metabolites. Samples can then be compared via their own measured profile.

### 2.9. Cytotoxicity (LDH-assay)

Calu-3 cells were seeded on transwell inserts (3460 Corning Costar, USA) with a cell count of  $10^5$  per well. Cells were cultured with 500  $\mu\text{l}$  medium apically and 1500  $\mu\text{l}$  basolaterally for 3 d. Then, cells were set up to air–liquid conditions with 500  $\mu\text{l}$  medium basolateral only for one week. Cell medium was exchanged every second day and quality control and confluence was monitored using bright field microscopy. LDH assay was performed after one week of culture under air–liquid conditions. Prior to the experiment, medium was exchanged. Biofilm bioinks prepared as described were used to directly print two layers of a 6  $\times$  6 mm non-porous structure on cells. Half of the samples were crosslinked for 15 min with 300  $\mu\text{l}$  100 mM CaCl<sub>2</sub> and then washed twice with PBS. The plain hydrogel without bacteria was printed equally on cells as control. TritonX treated cells served as a dead control and untreated cells as live control. After 6 and 24 h, 200  $\mu\text{l}$  of basolateral medium was transferred to an Eppendorf tube. LDH solution (Roche, Germany) was prepared according to manufacturer's protocol and 100  $\mu\text{l}$  of the collected medium were added quickly to 100  $\mu\text{l}$  of the solution in a 96-well plate. Absorbance was measured at 492 nm, from which toxicity was calculated.

To complement the LDH assay we also performed a Casy<sup>®</sup> cell counter (OMNI LIFE Science, Germany)

analysis to evaluate the viability accordingly, as further described in supporting information 3.5.

### 2.10. Fluorescent staining of printed biofilms and Calu-3 cells

To visualize that biofilms could be formed and controlled on human *in vitro* systems, they were printed thinly (<300  $\mu\text{m}$ ) in different shapes on Calu-3 cells. Calu-3 cells were grown to confluent monolayers on transwell inserts for one week under air–liquid conditions and stained just before the biofilm printing procedure. This was necessary, because the staining dyes are non-specific and could also stain the biofilms after printing, making it difficult to differentiate mammalian and bacterial cell structures. Therefore, cells were fixed with 300  $\mu\text{l}$  paraformaldehyde apically and basolaterally with 600  $\mu\text{l}$  for 1 h. Then, 300  $\mu\text{l}$  blocking buffer was added apically for 20 min. Fluorescence stains were added apically and incubation was performed at RT in the dark. The 300  $\mu\text{l}$  of 66  $\mu\text{M}$  rhodamine-phalloidin (540 nm excitation, red emission; Invitrogen<sup>™</sup>, USA), diluted 1:200 in blocking buffer (1% bovine serum albumin heat shock fraction and 0.05% Saponin (both Sigma Aldrich, Germany), in PBS) was added apically. Cells were stained for 1 h at RT in the dark. Cells were then washed twice with 300  $\mu\text{l}$  PBS. Next, 200  $\mu\text{l}$  of 5  $\mu\text{g ml}^{-1}$  DAPI (364 nm excitation, blue emission; Sigma-Aldrich, Germany) was added apically for 1 h in the dark. Dye solution was removed and 500  $\mu\text{l}$  PBS was added basolaterally to avoid cell drying.

In parallel, biofilms were stained. For that, 1.5  $\mu\text{l}$  of SYTO-9 dye from BacLight<sup>™</sup> was added into each of the 3 syringes after upper 4 ml were removed. Syringes were kept at 37 °C in the dark for 1 h. Then, the syringes were accordingly pooled and prepared for printing as described previously. Biofilms were then printed (1 layer) on top of stained cells in different shapes and immediately analyzed at the CLSM, using a 10 $\times$  objective (HC PL Fluotar 10 $\times$ /0.3 Dry, Leica, Germany) and the LAS X software. Z-stacks were collected of entire thickness from the cell layer and biofilms.

To assess shape retention, stained biofilms were also printed on unstained Calu-3 cell layers. Biofilms were then either crosslinked with 300  $\mu\text{l}$  CaCl<sub>2</sub> for 10 min with two PBS washing steps or not. Cells with biofilms were then cultured O/N in cell culture incubator and subsequently analyzed at the CLSM, using a 10 $\times$  objective (HC PL Fluotar 10 $\times$ /0.3 Dry, Leica, Germany) and the LAS X software.

For all images, triplicates were collected, each at 2–3 different and random *xyz* positions, providing a strong fluorescent signal.

### 2.11. Statistics

All experiments were performed in independent biological triplicates, each with technical triplicates

( $N = 3$ ;  $n = 9$ ), unless otherwise stated. Significance was checked for antibiotic susceptibility assays via one-way ANOVA with Tukey's multiple comparison tests. Statistical significance was defined as  $*p < 0.05$ ,  $**p < 0.01$ ,  $***p < 0.001$ . Error bars indicate standard deviation.

## 3. Results

### 3.1. Optimization of bioink

Firstly, we have developed a method for printing a pre-grown *E. coli* MG1655 biofilms, using a gelatin-alginate based bioink (figure 1). To determine the optimal gelatin-alginate (Gel;Alg) concentrations for the bioink, six different formulations (gelatin[% (w/v)];alginate[% (w/v)]: 2;1–4;2 as final concentration for bioink) were prepared equally. After testing bacterial growth in each candidate bioink, we observed comparable growth rates across all formulations (see supplement figure 1).

#### 3.1.1. Rheological properties and printability

All bioink candidates were analyzed rheologically and for their printing suitability. The results are summarized in figure 2 (gelatin[% (w/v)];alginate[% (w/v)]: 2;1, 3;1, 4;1) and supplement figure 2 (further tested gelatin-alginate concentrations showing same behavior provided in supplement). All samples showed viscoelastic solid behavior with  $G' > G''$  during frequency oscillation (figure 2(A), supplement figure 2(A)). Increasing polymer concentration showed higher  $G'$ , suggesting more mechanical strength/stiffness. Flow analysis showed shear-thinning behavior for all samples, demonstrated by decreasing viscosity with increasing shear rate (figure 2(B), supplement figure 2(B)). Higher polymer concentrations resulted in higher viscosity, suggesting again higher stiffness. Rheological properties were then complemented with printability properties. Filaments of all bioink candidates were extruded via air pressure. Visual observation of the droplet or filament extrusion process showed higher stiffness and gelation behavior for samples with higher polymer concentration. While 2;1 samples showed still droplet formation, the sample with 3;1 or higher polymer concentration former proper filaments (figure 2(C)). Accordingly, higher concentrations required more pressure to print the same constructs (figure 2(D), supplement table 1). To keep the air pressure as low as possible while still achieving proper filament extrusion, the 3;1 bioink was chosen for all further experiments. In addition, we also investigated the rheological properties and required extrusion pressure of the plain hydrogel (no bacteria) and with planktonic bacteria, which we used as controls. Rheological comparison showed higher mechanical stiffness of the plain hydrogel compared to both bioinks. Planktonic and biofilm bioink revealed also some differences, with planktonic bacteria showing higher mechanical

stiffness during frequency oscillation as well as higher required extrusion pressure (figures 2(E) and (F)).

#### 3.1.2. Printing variability: size and shape

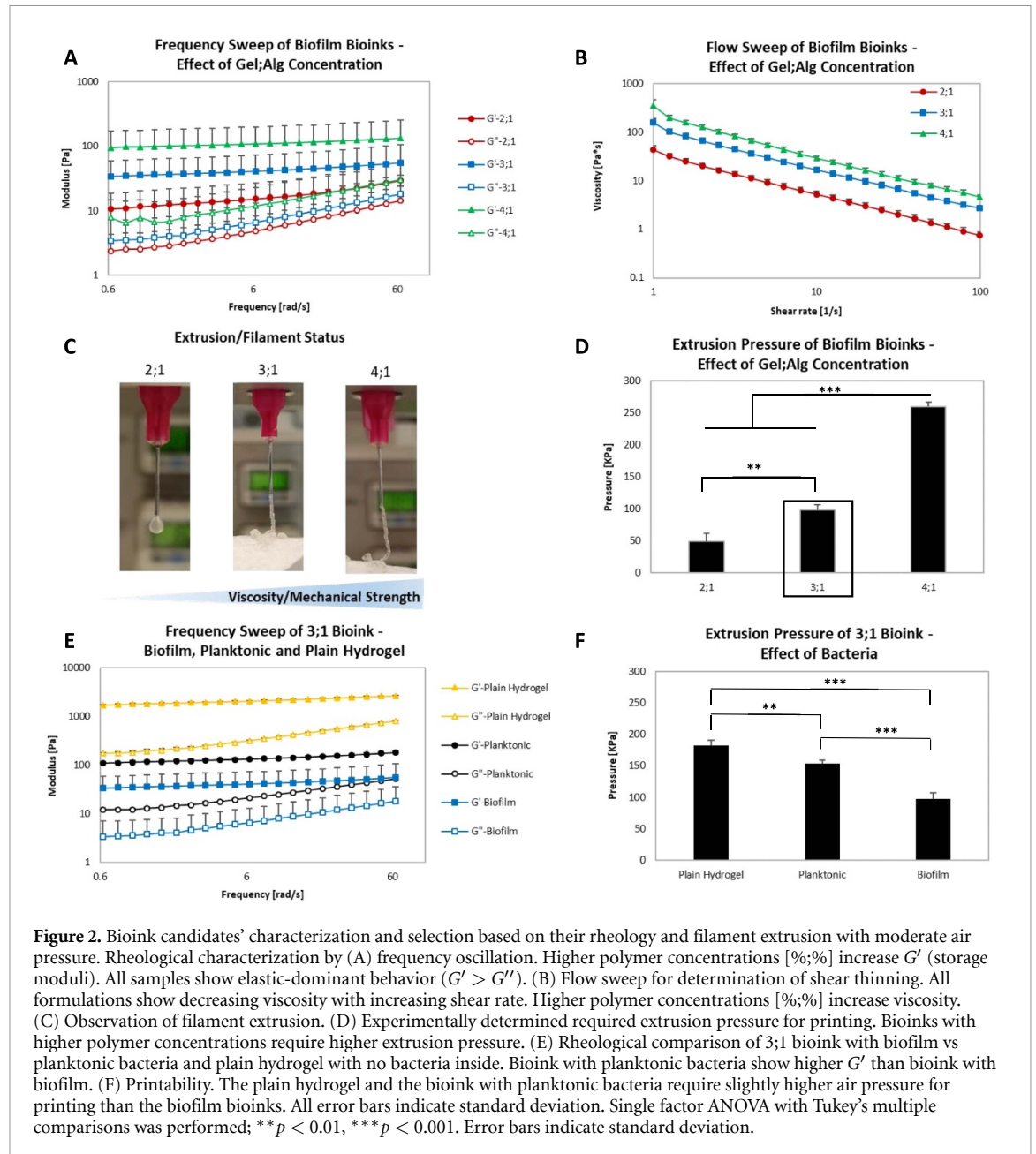
To exemplify design possibilities of bioprinting different constructs with varying shapes and dimensions were printed. Figure 3(A) shows printed biofilm samples of different thickness obtained by increasing the number of layers. Shape design for printing seems unlimited. We have chosen a grid and a star (figure 3(B)). As simplest proof of bacterial viability after printing, their growth was observed. We printed our institutes abbreviation HIPS with biofilm bioink on an agar plate. After incubating at 37 °C for one day, bacterial growth in the printed letters was visible, observed by appeared turbidity (figure 3(C)).

### 3.2. CLSM and SEM analysis of printed biofilm

To visualize bacteria and biofilm structures in the printed constructs, samples printed with planktonic bacteria and biofilm bacteria were subjected to CLSM and SEM. Two layered grids were printed and stained with the live/dead kit BacLight™ (SYTO9/propidium iodide) for CLSM analysis or dried for SEM analysis. The low propidium iodide staining in the printed planktonic construct confirms the macroscopic observation of high bacterial survival after printing (figure 4(A), left). Bioprinted planktonic bacteria showed homogeneously distributed single bacterial cells throughout the construct. The bioprinted biofilms showed as expected a morphology with different sizes of bacterial aggregations (figure 4(A), right). Clearly, the red signal from nucleic acid stain increased when comparing planktonic and biofilm bacteria. Similar observations were made when native biofilms were compared to native planktonic bacteria (supplement figure 3). The propidium iodide stains the nucleic acid inside of dead bacteria or dormant biofilms leaky membranes as well as extracellular DNA, which is a typical component of biofilm matrix. The three days growth in the bioink before printing allow biofilm production and natural cell death. Therefore, the higher red signal in the printed biofilm sample (figure 4(A)) might be rather attributed to the biofilm formation than the higher sensitivity to the printing process. SEM images confirmed the difference in bacterial cell distribution within the construct containing planktonic bacteria and biofilm. While planktonic bacteria were mostly single cells, the biofilm sample showed bacterial aggregates (figure 4(B)).

### 3.3. Antibiotic susceptibility of printed biofilms

A key feature for biofilm models in drug testing is their susceptibility against antibiotics. Therefore, we selected this property as readout to confirm maintenance of biofilm features after printing. Printed planktonic bacteria as well as native biofilms and native planktonic bacteria served as control. Comparability



of the models concerning their bacterial count was shown for untreated samples in each growth condition (supplement figure 3). Susceptibility against the four selected antibiotics is depicted as  $\Delta\text{Log}_{10}\text{CFU ml}^{-1}$ , calculated from the respective untreated controls (figure 5). Overall, susceptibility towards antibiotic treatment was more influenced by the planktonic or biofilm growth, than by the printing procedure. However, bioprinting requires the use of a bioink, which for some antibiotics seem to have an effect as well. For ampicillin, bioprinted biofilms and native biofilms showed no difference and were significantly more resistant than printed and native planktonics, which were completely eradicated. The selected tetracycline concentrations had rather moderate effects under all conditions. Both planktonic conditions as well as native biofilms showed no significant differences. Bioprinted biofilms were

significantly more resistant than the other conditions. Against colistin, bioprinted and native biofilms showed similar resistance and were significantly less sensitive than native planktonic bacteria. Although, no significant difference was seen towards biofilms, printed planktonic bacteria showed a more sensitive trend. The sample size  $n$  was increased from 9 to 15 for printed planktonic bacteria, but standard deviation was still quite high. A further increase of colistin concentration would have eradicated the biofilms (supplement figure 4). Finally, ciprofloxacin showed similar trends. However, biofilm conditions as well as printed planktonic bacteria were significantly more resistant than native planktonic bacteria. Printed and native biofilms showed again no significant difference. A trend to be more sensitive towards biofilms was shown again by printed planktonic bacteria, which was not significant.

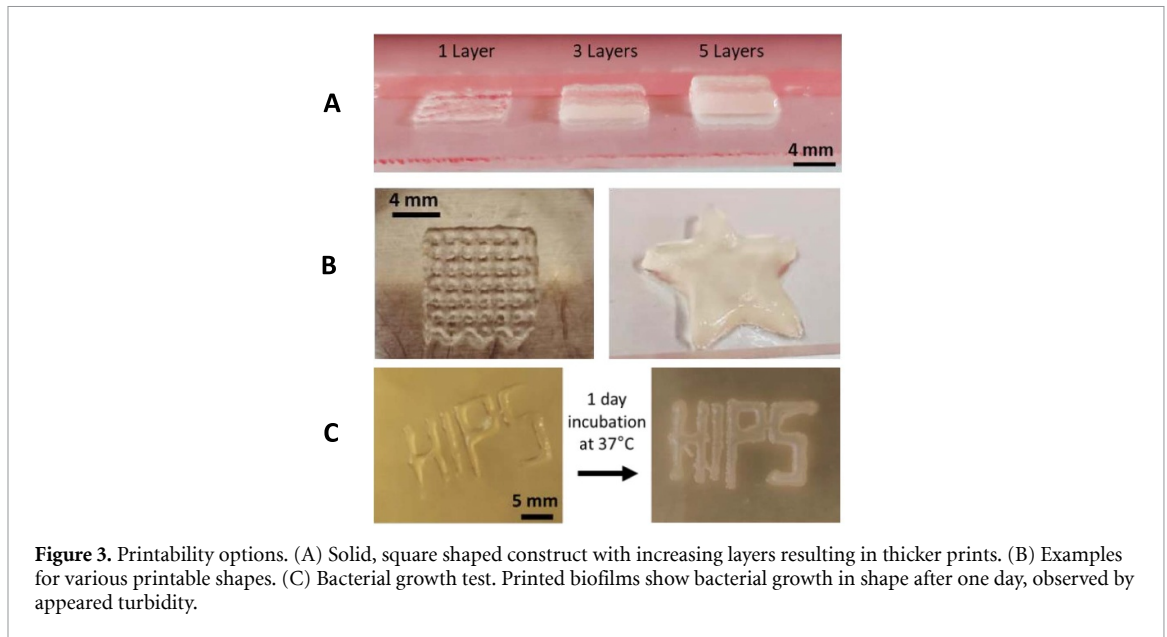


**Figure 3.** Printability options. (A) Solid, square shaped construct with increasing layers resulting in thicker prints. (B) Examples for various printable shapes. (C) Bacterial growth test. Printed biofilms show bacterial growth in shape after one day, observed by appeared turbidity.

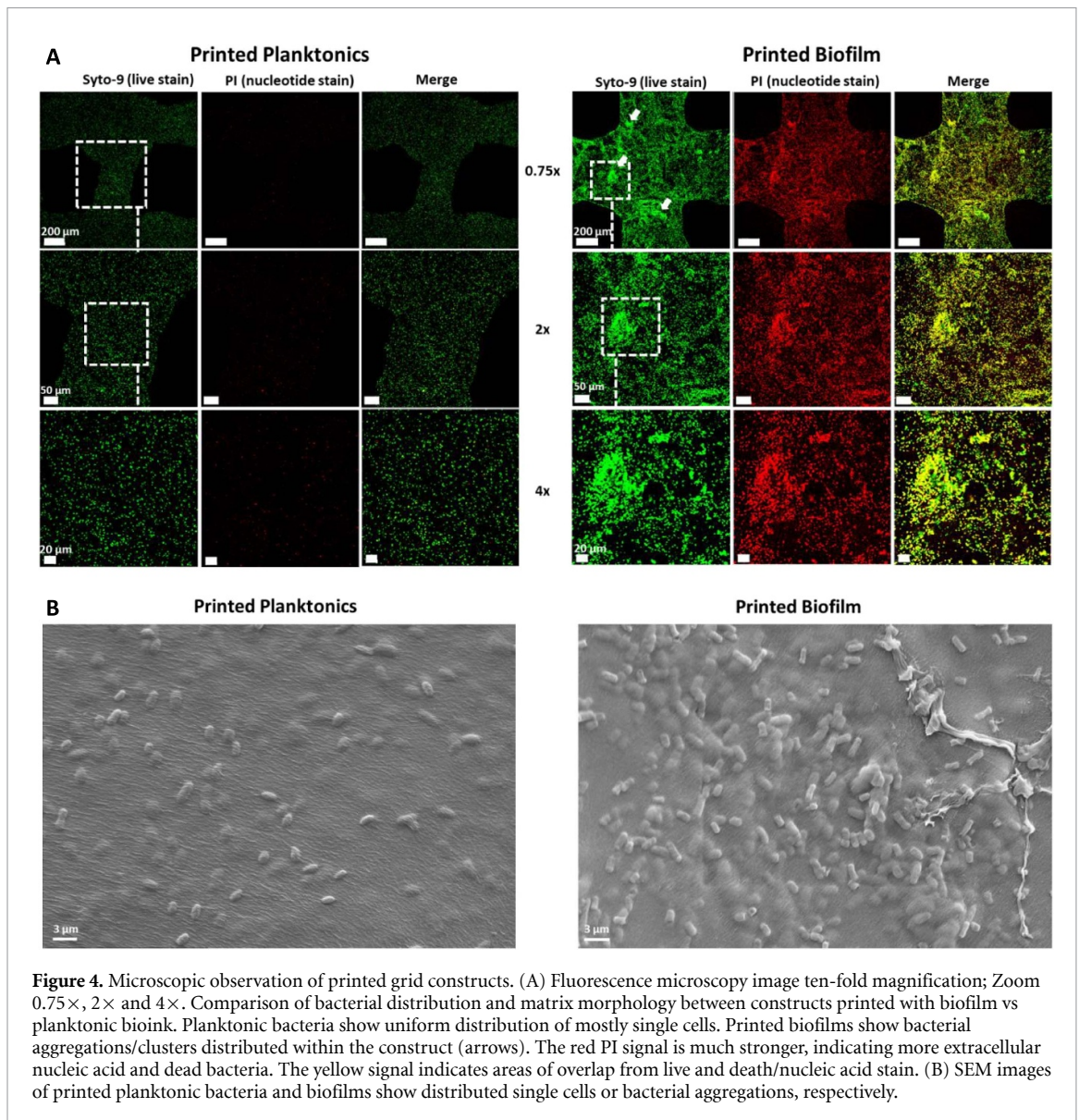


**Figure 4.** Microscopic observation of printed grid constructs. (A) Fluorescence microscopy image ten-fold magnification; Zoom 0.75×, 2× and 4×. Comparison of bacterial distribution and matrix morphology between constructs printed with biofilm vs planktonic bioink. Planktonic bacteria show uniform distribution of mostly single cells. Printed biofilms show bacterial aggregations/clusters distributed within the construct (arrows). The red PI signal is much stronger, indicating more extracellular nucleic acid and dead bacteria. The yellow signal indicates areas of overlap from live and death/nucleic acid stain. (B) SEM images of printed planktonic bacteria and biofilms show distributed single cells or bacterial aggregations, respectively.

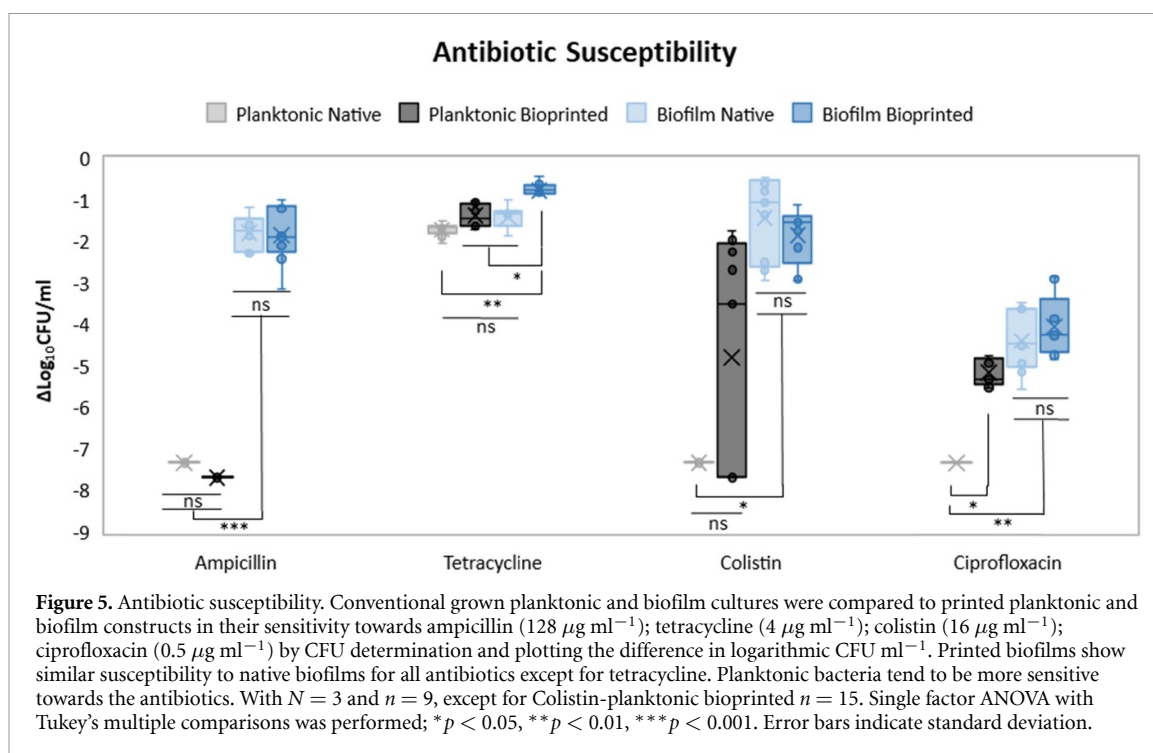


**Table 1.** Metabolic profile comparison of printed and native conditions.

Comparison	Specific features printed	Specific features native	Common features	Total feature	Similarity (%)
Planktonic printed—planktonic native	392	160	2104	2656	$79.2 \pm 3.6$
Biofilm printed—biofilm native	629	289	2113	3031	$69.7 \pm 4.4$

### 3.4. Metabolic profile analysis

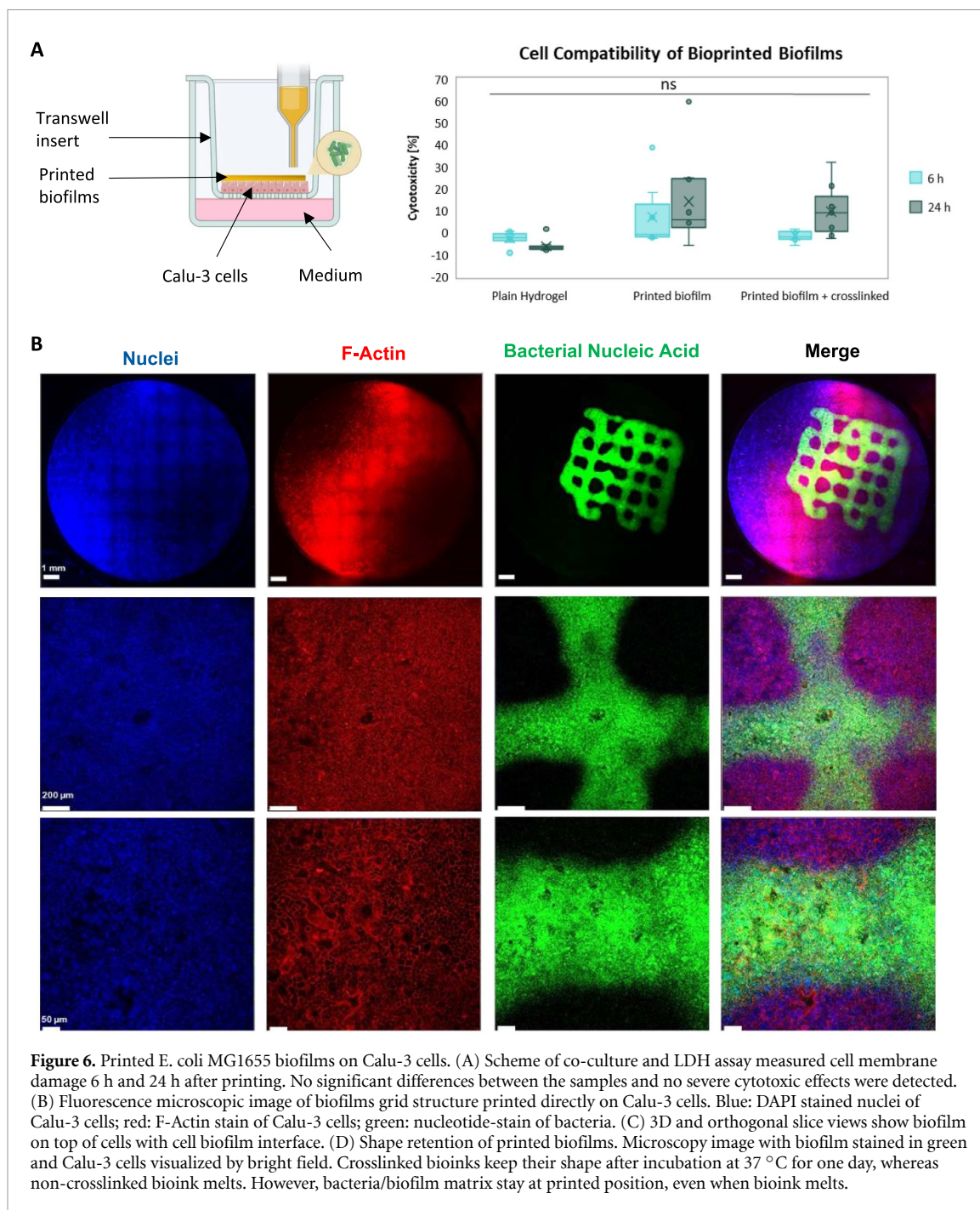
A broader indicator for biofilm behavior of bacteria is their metabolism, which we analyzed by LC-TOF measurements for the same four conditions, as described in the previous antibiotic susceptibility testing. To investigate the effect of printed bioinks to native conditions, we compared the entirety of all metabolic features from printed bacteria to their native counterpart (table 1). Specific features are metabolites present only in one condition, whereas common features show metabolites present in both compared conditions. Printed planktonic bacteria and planktonic native bacteria showed similarity of 79.2%, determined by the common and specific feature counts. A high similarity of 69.7% was found for printed and native biofilms too, indicating low impact on native metabolic state by bioprinting.

### 3.5. Bioprinting biofilms on Calu-3 cells

Calu-3 cells were selected as model human epithelial cell line to show that biofilms can be shaped by bioprinting directly on cell layers. Cells were grown at air-liquid conditions, which is quite common in such systems to mimic fundamental respiratory

epithelium aspects, but enables us also to deposit our bioinks on a substrate via bioprinting. Cytotoxicity analysis indicated that cells survive the printing process (figure 6(A)). The plain hydrogel without bacteria had no cytotoxic effects. Increased LDH release was measured for bioprinted biofilms crosslinked and non-crosslinked after 6 and 24 h (mean cytotoxicity carrying from 0% to 13%). However, there were no significant differences between the tested groups, indicating that the printing process has no relevant effect on cell integrity. To complement the LDH assay, a viability evaluation was performed with a Casy<sup>®</sup> cell counter, observing the same trend (supplement table 2). However, a slightly lower viability was shown for samples with printed bacteria on top.

Fluorescence microscopy images showed that biofilms could be printed in various shapes on cells (figure 6(B), supplement figure 5). The 3D image view and orthogonal slices showed direct contact of biofilm with the epithelial surface (figure 6(C)). Shape retention could be maintained when the bioink was crosslinked, whereas non-crosslinked bioink melted at  $37^\circ\text{C}$  during the 1 day incubation (figure 6(D)). However, no n-crosslinked biofilms



showed bacterial shape retention, which means that the bacterial biofilm matrix stayed at the printed position even when the bioink hydrogel melted. The letters of the crosslinked construct showed incomplete fluorescence signal, although visible in bright-field. This might be a result of different *Z*-planes of the letters due to the crosslinking procedure with inhomogeneous swelling and shrinking effects.

#### 4. Discussion

Here we report a novel approach for 3D printing of bacterial biofilms on human epithelial cell monolayers which is necessary for modeling biofilm related

infectious diseases under controlled conditions *in vitro*. Previous approaches for bioprinting biofilms relied on bioprinting of planktonic bacteria, converting slowly into biofilms after printing [15, 22]. However, this process could lead to premature death of the intended mammalian cell substrate. Therefore, we chose to print *E. coli* MG1655 that had already converted from the planktonic to the biofilm state after dispersion in a suitable gelatin-alginate bioink. The selected polymer concentrations of the bioink showed different rheology when printed with biofilms or planktonic bacteria, respectively. Upon conversion into biofilms, the bioinks showed less mechanical stiffness and required less

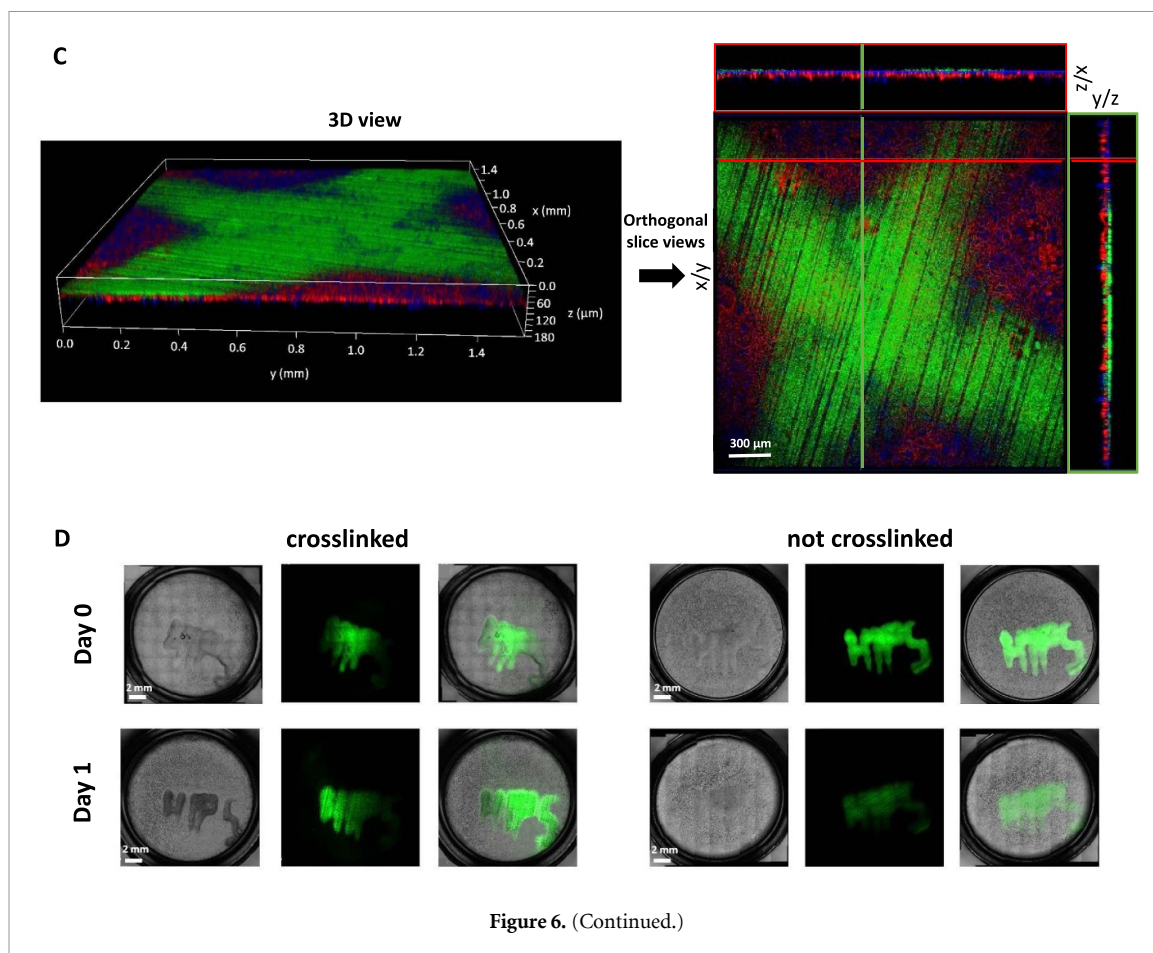


Figure 6. (Continued.)

printing pressure, which can be explained either by commencing polymer digestion after 3 d or by a release of rheodestructive components during biofilm formation [12]. Similarly, compared to the plain hydrogel, the planktonic bacteria also showed mechanical strength reduction, indicating an early induction of these processes. While no longer in planktonic, but already in biofilm state, the bacteria could now be printed in a wide range of dimensions and shapes. Flexibility of this approach is highly required for a variety of applications. Varying biofilm thickness could be applied to systematically study biofilm related infections. For example thicker biofilms up to 1000  $\mu\text{m}$  and beyond are found on implants, catheters or shunts. For skin wounds, lung infections or other tissues the upper size limit is around 200  $\mu\text{m}$  [29]. These ranges can be achieved by our approach, which might also be a suitable method to test anti-infectives on biofilms with different thicknesses. Shape flexibility might be of great interest to mimic specific biofilm forms, because *in vitro* native biofilms form mushroom shaped-structures, which are not common in *in vivo* biofilm infections [11, 30].

Biofilm morphology could be differentiated from printed planktonic bacteria as biofilms exhibited typical bacterial aggregations, spread in the prints [24]. The increased red signal due to increased presence of nucleic acid was expected, because the longer

incubation time can result in more dead bacteria. Another aspect is the option of dormant biofilms with leaky membranes potentially leading to double staining without cells actually being dead [31, 32]. But also, the release of nucleic acid during biofilm formation could enhance the stain. Extracellular DNA is a typical component of biofilm matrix. A differentiation of dead bacteria or nucleic acid release in ECM was not possible with our method. The merge image of the printed biofilm sample, however, shows colocalization of the green signal from the live-stain with red nucleic acid stain resulting in yellow dense clusters as they are anticipated for living bacteria shielding in biofilm matrix. SEM analyzed prints had to be gold-sputtered, which compromises the visibility of the hydrogel structures of the bioink, or bacteria produced ECM. Nevertheless, bacterial aggregates are still observed and are typical for the presence of a biofilm matrix [16, 33].

Antibiotic susceptibility assays indicated that printed biofilms behave similar as native biofilms. The four antibiotics operated differently. Ampicillin had the strongest effect under planktonic conditions, whereas printed and native biofilms showed higher resistance, which was expected, based on previous studies by Ito *et al* [34]. Tetracycline, known to be a bacteriostatic anti-infective, had a comparably low overall effect, but showed significantly higher

effects against printed planktonic and native planktonic bacteria as well as native biofilms than on printed biofilms. This difference of native and printed biofilms was rather unexpected, since it has been reported that tetracycline act more effectively on native biofilms than on planktonic bacteria [35, 36]. Colistin showed no significant difference between printed and native biofilms, but also did not exhibit significant difference towards printed planktonic bacteria. As a molecule with higher molecular weight, colistin may encounter difficulties in penetrating crosslinked hydrogels. Colistin had a stronger effect on native planktonic bacteria, which supports that hypothesis. Ciprofloxacin had a strong effect on all conditions. Again, no significant difference was found between printed and native biofilms. However, higher resistance of printed planktonic bacteria towards native planktonic bacteria was unexpected and could be attributed to the presence of calcium ions in the crosslinked prints. Ciprofloxacin is known to form chelate complexes with calcium and other metal ions [37], leading perhaps to lower effectivity in the printed planktonic bacteria. Overall, the printed biofilms showed high similarity of antibiotic resistance compared to native biofilms, indicating minimal influence on the ECM by printing.

Metabolic profile analysis showed close similarity of printed planktonic and biofilms towards their native counterpart. This suggests that the bioprinting process has only a minor impact on the metabolic state of bacteria. Although, the nutrition base was equal in all conditions, the polymer presence in the bioink could also influence the metabolism and should be considered. Since a metabolic reprogramming does occur in biofilms [38], a closer look into specific metabolic markers with suitable standards could be the subject of metabolomics-based follow-up studies, to compare the planktonic conditions to the biofilms. Genomic and proteomic technologies could give additional insight in this regard.

As a proof of concept, we printed bacterial biofilms on transwell-grown monolayers of human bronchial epithelial cells (Calu-3). We demonstrated cell compatibility of the bioink. Although, crosslinking of bioinks had no direct cytotoxic effects, the addition of  $\text{CaCl}_2$  could activate undesired signal cascades of cells, which needs to be considered. The slight increase of LDH from 6 h to 24 h indicates that the cause is more likely bacterial rather than the printing procedure. Moreover, other strains and pathogens might harm the cells in a much greater magnitude. As shape retention is also an important aspect for this approach, we demonstrated, that crosslinking printed biofilms on cells can keep their shape at least for one day at 37 °C. Ning *et al* showed that stability of crosslinked prints could be controlled via crosslinking time,  $\text{CaCl}_2$  concentration or via  $\text{BaCl}_2$  [28]. Nevertheless, the ECM as produced by the bacteria seems to keep the shape at air-liquid condition also

when not crosslinked, even when the bioink melts. This indicates that crosslinking is maybe not necessary to maintain biofilm shape, which could be beneficial when shaping the pure biofilm is required. Furthermore, the direct contact of biofilms with epithelial cells showed more similarities to what actually occurs *in vivo* compared to animal models, using bacteria loaded agar beads [22].

As mentioned previously, current approaches of biofilm infected human *in vitro* model still lack in controllability and reproducibility of biofilm transfer. We showed that 3D bioprinting of biofilms on epithelial cell layer can overcome these limitations. Taking the benefits of our method into account, the approach may be further adapted to other clinically relevant strains like *P. aeruginosa* or *S. aureus*, which might however need a tailored approach for bioinks to satisfy nutritional demands and withstand catalytic bacterial enzymes. However, such strains could potentially be more harmful to the host cells when leaving the printed biofilm matrix, which needs to be considered. Finally, the goal is to develop human-relevant *in vitro* infection models comprising biofilms of defined shape and metabolic status, which can be reproducibly produced and controlled over a longer period of time. This implies that the model should enable repeated drug administration and have the potential to sustain these 'co-cultures' not just for a few days, but for over a week. Complex models like these would allow to generate readouts for both the pathogens and the host cells to better predict the efficacy as well as the safety of tested drugs against biofilm infections.

## 5. Conclusion

We have successfully developed an innovative approach to bioprint biofilms on human epithelial cell layers. A gelatin-alginate based bioink was optimized to print *E. coli* MG1655 biofilm in various shapes and sizes, while retaining biofilm properties. Our method can be applied for multiple analytic options to characterize and evaluate biofilm status, including morphology, antibiotic susceptibility or metabolism. We showed a novel application of directly shaped biofilms on top of Calu-3 cell layer to demonstrate the control potential of *in vitro* biofilm infections. This method could pave the way to establish more robust human based *in vitro* models to test and optimize anti-infective strategies against biofilm related diseases.

## Data availability statement

The data cannot be made publicly available upon publication because they are not available in a format that is sufficiently accessible or reusable by other researchers. The data that support the findings of this

study are available upon reasonable request from the authors.

## Acknowledgments

This project received funding by the SET (Stiftung zur Förderung der Erforschung von Ersatz- und Ergänzungsmethoden zur Einschränkung von Tierversuchen, Frankfurt, Germany) and the Saarland University TANDEM graduate school. Pascal Paul and Annette Boese are thanked for technical support. The graph in figure 1 was created using [www.biorender.com](http://www.biorender.com).

## Author contributions

Conceptualization, S A, A H, B L and C-M L; Data curation, S A, S F, and N F; Supervision, A H, U F S, T V, B L and C-M L; Writing original Draft, S A; Writing-review and editing, S A, A H, S F, N F, D K, R M, U F S, T V, B L, and C-M L.

All authors have read and agreed to the published version of the manuscript.

## Conflict of interest

The authors declare no conflicts of interest.

## ORCID iDs

Samy Aliyazdi  <https://orcid.org/0009-0007-4141-5623>

Sarah Frisch  <https://orcid.org/0000-0003-2149-580X>

Alberto Hidalgo  <https://orcid.org/0000-0003-2090-7817>

Nicolas Frank  <https://orcid.org/0000-0001-7170-2366>

Daniel Krug  <https://orcid.org/0000-0002-3664-1884>

Rolf Müller  <https://orcid.org/0000-0002-1042-5665>

Ulrich F Schaefer  <https://orcid.org/0000-0002-2470-2168>

Thomas Vogt  <https://orcid.org/0000-0002-2824-5005>

Brigitta Loretz  <https://orcid.org/0000-0003-0057-5181>

Claus-Michael Lehr  <https://orcid.org/0000-0002-5864-8462>

## References

- Brinkman C L, Schmidt-Malan S M, Karau M J, Greenwood-Quaintance K, Hassett D J, Mandrekar J N and Patel R 2016 Exposure of bacterial biofilms to electrical current leads to cell death mediated in part by reactive oxygen species *PLoS One* **11** e0168595
- Wolcott R D, Rhoads D D, Bennett M E, Wolcott B M, Gogokhia L, Costerton J W and Dowd S E 2010 Chronic wounds and the medical biofilm paradigm *J. Wound Care* **19** 45–53
- Bjarnsholt T 2013 The role of bacterial biofilms in chronic infections *APMIS Suppl.* **121** 1–51
- Sharma D, Misba L and Khan A U 2019 Antibiotics versus biofilm: an emerging battleground in microbial communities *Antimicrob. Resist. Infect. Control* **8** 76
- Singh A, Amod A, Pandey P, Bose P, Pingali M S, Shivalkar S, Varadwaj P K, Sahoo A K and Samanta S K 2022 Bacterial biofilm infections, their resistance to antibiotics therapy and current treatment strategies *Biomed. Mater.* **17** 022003
- Kolpen M et al 2022 Bacterial biofilms predominate in both acute and chronic human lung infections *Thorax* **77** 1015–22
- Singh R, Sahore S, Kaur P, Rani A and Ray P 2016 Penetration barrier contributes to bacterial biofilm-associated resistance against only select antibiotics, and exhibits genus-, strain- and antibiotic-specific differences *Pathog. Dis.* **74** ftw056
- Guzmán-Soto I, McTiernan C, Gonzalez-Gomez M, Ross A, Gupta K, Suuronen E J, Mah T-F, Griffith M and Alarcon E I 2021 Mimicking biofilm formation and development: recent progress in *in vitro* and *in vivo* biofilm models *iScience* **24** 102443
- Folkesson A, Jelsbak L, Yang L, Johansen H K, Ciofu O, Høiby N and Molin S 2012 Adaptation of *Pseudomonas aeruginosa* to the cystic fibrosis airway: an evolutionary perspective *Nat. Rev. Microbiol.* **10** 841–51
- Høiby N, Ciofu O and Bjarnsholt T 2010 *Pseudomonas aeruginosa* biofilms in cystic fibrosis *Future Microbiol.* **5** 1663–74
- Lebeaux D, Chauhan A, Rendueles O and Beloin C 2013 From *in vitro* to *in vivo* models of bacterial biofilm-related infections *Pathogens* **2** 288–356
- Anderson G G, Moreau-Marquis S, Stanton B A and O'Toole G A 2008 *In vitro* analysis of tobramycin-treated *Pseudomonas aeruginosa* biofilms on cystic fibrosis-derived airway epithelial cells *Infect. Immun.* **76** 1423–33
- Woodworth B A, Tamashiro E, Bhargava G, Cohen N A and Palmer J N 2008 An *in vitro* model of *Pseudomonas aeruginosa* biofilms on viable airway epithelial cell monolayers *Am. J. Rhinol.* **22** 235–8
- Bowler L L, Ball T B and Seward L L 2014 A novel *in vitro* co-culture system allows the concurrent analysis of mature biofilm and planktonic bacteria with human lung epithelia *J. Microbiol. Methods* **101** 49–55
- Montefusco-Pereira C V, Horstmann J C, Ebensen T, Beisswenger C, Bals R, Guzmán C A, Schneider-Daum N, Carvalho-Wodarz C D S and Lehr C-M 2020 *P. aeruginosa* infected 3D co-culture of bronchial epithelial cells and macrophages at air-liquid interface for preclinical evaluation of anti-infectives *J. Vis. Exp.* **160**
- Horstmann J C et al 2022 Transferring microclusters of *P. aeruginosa* biofilms to the air-liquid interface of bronchial epithelial cells for repeated deposition of aerosolized tobramycin *ACS Infect. Dis.* **8** 137–49
- Juntke J, Murgia X, Günday Türeli N, Türeli A E, Thorn C R, Schneider M, Schneider-Daum N, de Souza Carvalho-wodarz C and Lehr C M 2021 Testing of aerosolized ciprofloxacin nanocarriers on cystic fibrosis airway cells infected with *P. aeruginosa* biofilms *Drug Deliv. Transl. Res.* **11** 1752–65
- Gao G, Schilling A F, Yonezawa T, Wang J, Dai G and Cui X 2014 Bioactive nanoparticles stimulate bone tissue formation in bioprinted three-dimensional scaffold and human mesenchymal stem cells *Biotechnol. J.* **9** 1304–11
- Noor N, Shapira A, Edri R, Gal I, Wertheim L and Dvir T 2019 3D printing of personalized thick and perfusable cardiac patches and hearts *Adv. Sci.* **6** 1900344
- Mirdamadi E, Tashman J W, Shiwarski D J, Palchesko R N and Feinberg A W 2020 FRESH 3D bioprinting a full-size model of the human heart *ACS Biomater. Sci. Eng.* **6** 6453–9
- Taymour R, Kilian D, Ahlfeld T, Gelinsky M and Lode A 2021 3D bioprinting of hepatocytes: core-shell structured

- co-cultures with fibroblasts for enhanced functionality *Sci. Rep.* **11** 5130
- [22] Baltazar T et al 2020 Three dimensional bioprinting of a vascularized and perfusable skin graft using human keratinocytes, fibroblasts, pericytes, and endothelial cells *Tissue Eng. A* **26** 227–38
- [23] Ozbolat I T, Peng W and Ozbolat V 2016 Application areas of 3D bioprinting *Drug Discov. Today* **21** 1257–71
- [24] Schaffner M, Rühls P A, Coulter F, Kilcher S and Studart A R 2017 3D printing of bacteria into functional complex materials *Sci. Adv.* **3** eaa06804
- [25] Dubbin K et al 2021 Projection microstereolithographic microbial bioprinting for engineered biofilms *Nano Lett.* **21** 1352–9
- [26] Spiesz E M, Yu K, Lehner B A E, Schmieden D T, Aubin-Tam M-E and Meyer A S 2019 Three-dimensional patterning of engineered biofilms with a do-it-yourself bioprinter *J. Vis. Exp.* **147**
- [27] Balasubramanian S, Yu K, Cardenas D V, Aubin-Tam M-E and Meyer A S 2021 Emergent biological endurance depends on extracellular matrix composition of three-dimensionally printed *Escherichia coli* biofilms *ACS Synth. Biol.* **10** 2997–3008
- [28] Ning E, Turnbull G, Clarke J, Picard F, Riches P, Vendrell M, Graham D, Wark A W, Faulds K and Shu W 2019 3D bioprinting of mature bacterial biofilms for antimicrobial resistance drug testing *Biofabrication* **11** 045018
- [29] Bjarnsholt T, Alhede M, Alhede M, Eickhardt-Sørensen S R, Moser C, Kühl M, Jensen P Ø and Høiby N 2013 The *in vivo* biofilm *Trends Microbiol.* **21** 466–74
- [30] Ghanbari A, Dehghany J, Schwebs T, Müsken M, Häussler S and Meyer-Hermann M 2016 Inoculation density and nutrient level determine the formation of mushroom-shaped structures in *Pseudomonas aeruginosa* biofilms *Sci. Rep.* **6** 32097
- [31] Chihara K, Matsumoto S, Kagawa Y and Tsuneda S 2015 Mathematical modeling of dormant cell formation in growing biofilm *Front. Microbiol.* **6** 534
- [32] Zou J, Peng B, Qu J and Zheng J 2021 Are bacterial persisters dormant cells only? *Front. Microbiol.* **12** 708580
- [33] Ansari M A, Khan H M, Khan A A, Cameotra S S and Pal R 2014 Antibiofilm efficacy of silver nanoparticles against biofilm of extended spectrum  $\beta$ -lactamase isolates of *Escherichia coli* and *Klebsiella pneumoniae* *Appl. Nanosci.* **4** 859–68
- [34] Ito A, Taniuchi A, May T, Kawata K and Okabe S 2009 Increased antibiotic resistance of *Escherichia coli* in mature biofilms *Appl. Environ. Microbiol.* **75** 4093–100
- [35] Stone G, Wood P, Dixon L, Keyhan M and Matin A 2002 Tetracycline rapidly reaches all the constituent cells of uropathogenic *Escherichia coli* biofilms *Antimicrob. Agents Chemother.* **46** 2458–61
- [36] Hu X, Zhang Y, Chen Z, Gao Y, Teppen B, Boyd S A, Zhang W, Tiedje J M and Li H 2023 Tetracycline accumulation in biofilms enhances the selection pressure on *Escherichia coli* for expression of antibiotic resistance *Sci. Total Environ.* **857** 159441
- [37] El-Sabawi D, Abu-Dahab R, Zalloum W A, Ijbara F and Hamdan I I 2019 The effect of ferrous ions, calcium ions and citric acid on absorption of ciprofloxacin across CaCo-2 cells: practical and structural approach *Drug Dev. Ind. Pharm.* **45** 292–303
- [38] Guo R, Luo X, Liu J and Lu H 2021 Mass spectrometry based targeted metabolomics precisely characterized new functional metabolites that regulate biofilm formation in *Escherichia coli* *Anal. Chim. Acta* **1145** 26–36